Nonlinear Analysis of Composite Steel Girder Bridges

LINZHONG DENG and MICHEL GHOSN

ABSTRACT

This paper describes a procedure for the nonlinear analysis of composite steel girder highway bridges. The procedure uses a modified grillage (grid) analysis method where material nonlinearity is modeled by empirically derived moment-curvature relationships. These are obtained from experimental data on the behavior of typical composite steel girder bridges. A linear variation of plastic curvature along the length of each beam element is assumed. An equivalent grid plastic hinge length, L_{gp}, is used to simulate the extent of plastification over the whole length of a grid element. The procedure can account for span continuity by including a negative bending moment-curvature relationship. Numerical investigations verify the proposed method's validity by comparing the analytical results with those of in-situ and laboratory full-scale and model-scale bridge tests. This paper also demonstrates that the proposed nonlinear analysis method provides a simple tool that can be used to obtain reasonably accurate representations of the nonlinear behavior of composite steel girder bridges. The method uses a grillage discretization technique whose results are relatively insensitive to variations in the mesh size. The proposed method has a high potential for use in engineering practice because of the simple input requirements and its reasonable level of accuracy.

INTRODUCTION

The stiffness matrix method, and particularly the grillage analysis approach, has been widely used for several decades to perform the linear-elastic structural analysis of buildings and bridge systems. The grillage method is currently the most widely used approach in bridge engineering practice. For example, the AASHTO-LRFD Specifications (AASHTO, 1994) propose a set of empirical equations for calculating the girder distribution factors. These equations were obtained based on the grillage analysis of typical bridge configurations (Zokaie, Osterkamp, and Imbsen, 1991). In addition, the Specifications recommend that engineers perform their own analyses using either the grillage method or more refined finite element methods to obtain more accurate results. In Europe, where bridge design specifications do not provide load distribution factors, bridge engineers often perform a grillage-type analysis to predict the distribution of the applied forces to individual bridge members and to evaluate the safety of their designs (Hambly, 1991).

Traditional grillage analysis consists of modeling a bridge superstructure as a grid formed by linear elastic beam elements. The longitudinal members of the bridge system are modeled as longitudinal beam elements along the main axis of the bridge, while the slab and diaphragms are modeled as transverse beams. This approach is used for slab bridges, composite and non-composite slab on girder bridges as well as spread box beam bridges and multi-cell box bridges (Hambly, 1991).

Most applications of the grillage method in bridge analysis are based on the linear elastic stiffness matrix approach although researchers have adopted it to nonlinear analysis by updating the stiffness matrix at every load increment to reflect the reduced stiffness that occurs when portions of a beam plasticize. Another method assumes that the plastic zone is concentrated at the ends of each beam element where plastic hinges would form (Livesley, 1970). The typical application of this method for the nonlinear analysis of bridge systems has been described by Ghosn, Casas, and Xu (1996) and Ricles and Popov (1994). In the latter reference, the hinge at each end of the beam element is divided into a series of subhinges as illustrated in Figure 1. The formulation of the nonlinear stiffness matrix of a beam element is based on the assumption that the linear elastic section of the beam is in series with the nonlinear hinge at each of its ends (nodes I and J, as shown in Figure 1). Inelastic flexural and shear deformations developed in the flexural and shear subhinges, in addition to the elastic flexural and shear deformations of the beam itself, give the total deformation of the nonlinear beam. Each hinge is of zero length, and consists of a number of subhinges (for example, eight subhinges are shown in Figure 1). Hence most of the beam remains in the elastic range. Each subhinge has a rigid plastic force-deformation relationship. In the linear elastic range, the subhinges at the ends of the beam are rigid (have an infinite stiffness). Therefore, the element stiffness is that of the elastic beam alone. As the loads applied on the structure

Linzhong Deng is graduate research assistant, Department of Civil Engineering, City College of New York and graduate center of the City University of New York, CUNY, New York, NY.

Michel Ghosn is professor of Civil Engineering, City College of New York, CUNY, New York, NY.

increase beyond the elastic limit, the subhinges yield one by one. A reduction in the total element stiffness occurs due to the softening of the stiffnesses of the subhinges. The relationship between the deformations of each hinge (the assembly of the subhinges) and the element's end generalized forces (shear forces and moments) can be represented by multi-linear curves as shown in Figure 2. The focus of this paper is on the nonlinear behavior in bending although the nonlinear behavior of beam elements under shear deformations can also be included as demonstrated by Ricles and Popov (1994) and Ghosn, Casas, and Xu (1996).

The effect of the plastic subhinges is modeled as rotational springs connected to the ends of the elastic beams. Details on the derivation of the stiffness matrix of beam elements with ends connected to plastic rotational springs are given by Livesley (1970), Ghosn, Casas, and Xu (1996) and Ricles, Yang, and Priestley (1998). As an example, the grillage element stiffness matrix for the element shown in Figure 1 can be expressed as shown in Figure 3. The stiffness matrix shown in Figure 3 assumes uncoupling between the torsional stiffness and the bending stiffness of the beam element at all load levels and assumes a linear elastic behavior in torsion. The nonlinear effects are represented by the slopes of the plastic M-θ curve for each element. These curves model the nonlinear behavior of composite steel members as explained in the next section.

MODELING THE NONLINEAR BEHAVIOR OF COMPOSITE STEEL MEMBERS

The factors affecting the nonlinear behavior of composite steel members are complex and intricately interrelated. Local flange, local web and lateral-torsional distortions interact and tend to build up gradually. Experimental inves-

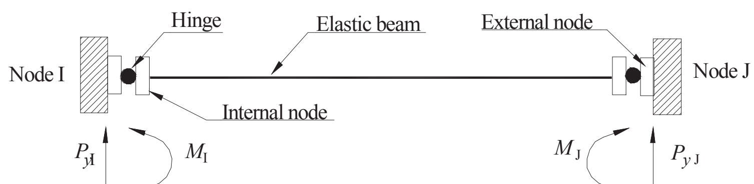

(a) Beam model

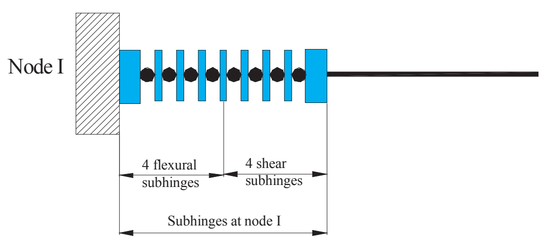

(b) Hinge model

Fig. 1. Nonlinear representation of bridge beam elements.

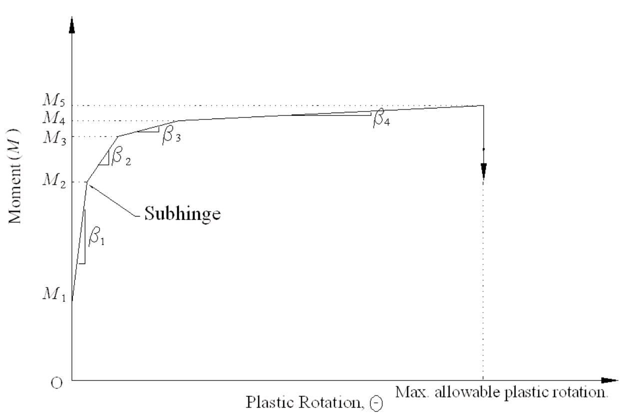

(a) Moment vs. plastic rotation curve

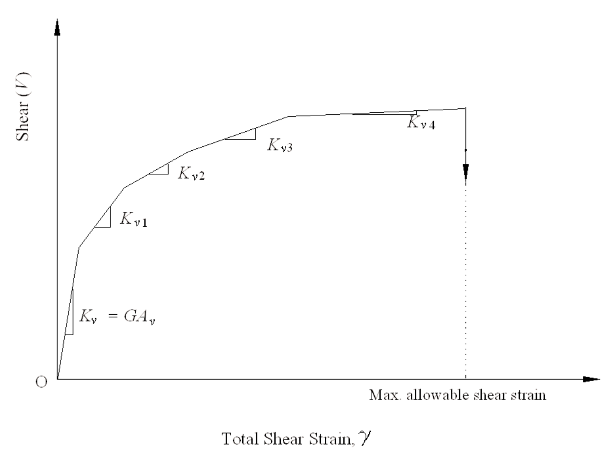

(b) Shear force vs. shear strain curve

Fig 2. Idealized force-deformation relationships of nonlinear hinges.

tigations have shown that composite sections begin to exhibit nonlinear behavior at a relatively small load that is about 20 percent of the ultimate capacity. This is believed to be due to the residual stresses in the beams, the effect of the shear connectors, the nonlinear properties of the concrete and the reinforcing steel. Beyond this range, strain hardening and instability work against each other and tend to balance out (Schilling and Morcos, 1988; Vasseghi and Frank, 1987).

Several researchers have attempted to develop analytical models to study the general behavior of composite steel girder bridges (Razaqpur and Nofal, 1988; Komatsu, Moriwaki, Fujino, and Takimoto, 1984; Idriss and White, 1991; Hall and Kostem, 1981). Other researchers gave special attention to the particular factors influencing the behavior of composite steel sections. For example, Keuser and Mehlborn (1987) developed a model that considers the effect of reinforcement bonding. Razaqpur and Nofal (1988), Kullman and Hosain (1985) and Hawkin and Mitchell (1984) presented models to describe the effects of shear connectors. Nagarajarao, Estuar, and Tall (1964) gave models for the residual stresses in steel members. Zdenek, Bazant, and Byung (1983) studied the effect of concrete cracking. These models can then be included in a detailed finite element analysis to study the behavior of composite steel bridges. However, these methods are difficult to use in practice because they either require large computational effort or demand detailed data that is often hard to obtain as many of the required parameters need to be determined on a case by case basis. For these reasons, developing a simple yet accurate method that can be applied on a routine basis is deemed to be of utmost importance.

This paper proposes a method to represent the nonlinear behavior of bridge elements by evenly spreading the effects

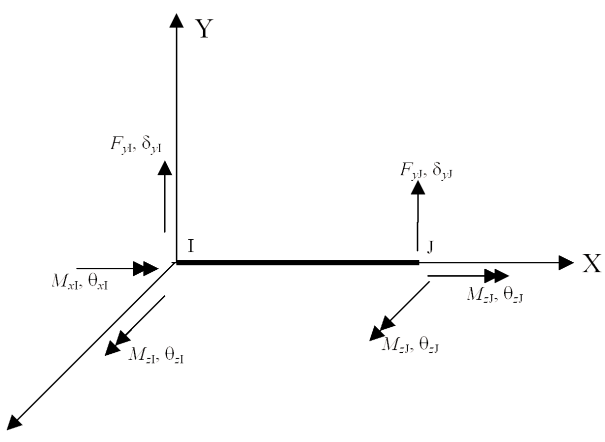

(a) Local coordinates system

$$\begin{bmatrix} F_{yI} \\ M_{xI} \\ M_{zI} \\ F_{yJ} \\ M_{xJ} \\ M_{zJ} \end{bmatrix} = \begin{bmatrix} K_{1,1} & 0 & K_{1,3} & K_{1,4} & 0 & K_{1,6} \\ 0 & K_{2,2} & 0 & 0 & K_{2,5} & 0 \\ K_{3,1} & 0 & K_{3,3} & K_{3,4} & 0 & K_{3,6} \\ K_{4,1} & 0 & K_{4,3} & K_{4,4} & 0 & K_{4,6} \\ 0 & K_{5,2} & 0 & 0 & K_{5,5} & 0 \\ K_{6,1} & 0 & K_{6,3} & K_{6,4} & 0 & K_{6,6} \end{bmatrix} \begin{bmatrix} \delta_{xI} \\ \theta_{xI} \\ \theta_{zI} \\ \delta_{yJ} \\ \theta_{xJ} \\ \theta_{zJ} \end{bmatrix}$$

$$K(1,1) = K(4,4) = 6\left[-1 + \frac{3(2+C_1)(2+C_2)}{C_1(4+C_2)+4(3+C_2)}\right]\frac{EI_z}{L^3}$$

$$K(1,3) = K(3,1) = \frac{6(2+C_2)}{C_1(4+C_2)+4(3+C_2)}\frac{\beta_1}{L}$$

$$K(1,4) = K(4,1) = 6\left[1 - \frac{3(2+C_1)(2+C_2)}{C_1(4+C_2)+4(3+C_2)}\right]\frac{EI_z}{L^3}$$

$$K(1,6) = K(6,1) = \frac{6C_2(2+C_1)}{C_1(4+C_2)+4(3+C_2)}\frac{EI_z}{L^2}$$

$$K(3,3) = \frac{4(3+C_2)\beta_1}{C_1(4+C_2)+4(3+C_2)}$$

$$K(3,6) = K(6,3) = \frac{2C_1C_2}{C_1(4+C_2)+4(3+C_2)}\frac{EI_z}{L}$$

$$K(4,6) = K(6,4) = -K(1,6)$$

$$K(3,6) = K(6,3) = \frac{2C_1C_2}{C_1(4+C_2)+4(3+C_2)}\frac{EI_z}{L}$$

$$K(6,6) = \frac{4(3+C_1)\beta_2}{C_1(4+C_2)+4(3+C_2)}$$

$$K(2,2) = K(5,5) = -K(2,5) = -K(5,2) = \frac{GJ_x}{L}$$

Where:

$$C_1 = \frac{\beta_I L}{EI_z}; \quad C_2 = \frac{\beta_J L}{EI_z}$$

β_I = slope of plastic M-θ curve for end I
β_J = slope of plastic M-θ curve for end J
J_x = torsional moment inertia x-axis
I_z = moment inertia about z-axis
L = the element length
E = elastic modulus
G = shearing modulus

(b) Stiffness matrix of one beam element

Fig. 3. Stiffness matrix of bridge beam element.

of nonlinearity over an equivalent grid element plastic hinge length, L_{gp}. The proposed method is empirical in the sense that it requires the availability of a "representative" moment-rotation curve. Such curves have been obtained through previous research studies at American Iron and Steel Institute (AISI) and the University of Texas (Vasseghi and Frank, 1987). The research sponsored by AISI has concluded that the nonlinear behavior of typical steel bridge sections can be modeled by moment versus plastic rotation curves similar to the Texas curve shown in Figure 4 (Schilling and Morcos, 1988). The Texas curve, obtained experimentally is normalized as a function of the ultimate plastic moment capacity, M_p. It describes the behavior of composite girders in positive bending. Curves for negative bending of beams with different section slenderness ratios are also available in the literature (Schilling, 1989). To obtain the curve of Figure 4, a 40-ft simple span beam was loaded by one concentrated force at the center. A portion of the total load was applied to the steel section before the slab hardened. Although the curve was obtained from a 40-ft beam, researchers at the University of Texas and AISI have shown that this curve models the behavior of most typical bridge sections for all span lengths (Vasseghi and Frank, 1987).

The Texas curve accounts for all the important factors that affect a composite steel section's nonlinear behavior including the effects of residual stresses, strain hardening, flexibility of shear connectors, effective slab width, effect of the slab's reinforcing steel and the cracking of the concrete slab. This curve will be used in the rest of this paper as the basic tool to describe any composite section's nonlinear properties in positive bending.

M-φ CURVE FOR POSITIVE BENDING OF STEEL BEAM SECTIONS

To execute the nonlinear grillage analysis, the stiffness matrix shown in Figure 3 must be evaluated at every load increment. In addition to the linear elastic properties of each beam element (moment of inertia I_z, elastic modulus E, polar inertia J_x and shear modulus G), assembling the stiffness matrix requires the determination of the element's rotational stiffnesses at both ends. These rotational stiffnesses are labeled, β_I and β_J, for ends I and J respectively.

The Texas curve cannot be directly used because the loading conditions and the support conditions of each element are different than those used to develop the Texas M-θ curve. However, the experimental curve contains the necessary information that can be utilized to obtain the required β_I and β_J coefficients. The procedure used in this study to obtain these coefficients consists of three steps:

1. Derive the moment-curvature relationship implicit in the Texas M-θ curve.
2. Discretize any other loaded beam into a number of elements and calculate the plastic rotation in the beam through a numerical integration of the curvature equation derived in step 1.
3. Calculate the plastic hinge stiffnesses β_I and β_J.

These steps are further described in the next sections. Details of the procedures and derivations are provided in Appendix A.

Derivation of Moment-Curvature Relationship

The end rotations of a beam element are related to the curvatures along the length of the element. These curvatures are themselves related to the internal bending moments. Therefore, determining the appropriate moment-curvature, M-φ, relationship is a very important factor for producing accurate results for the nonlinear behavior of bridge systems.

It is assumed that each composite steel section's plastic moment curvature relationship (M-φ curve) can be represented by a multilinear curve. It is also assumed that a typical loaded beam element IJ can be represented as shown in Figure 5 where θ_{TI} is the total rotation of the beam at end I

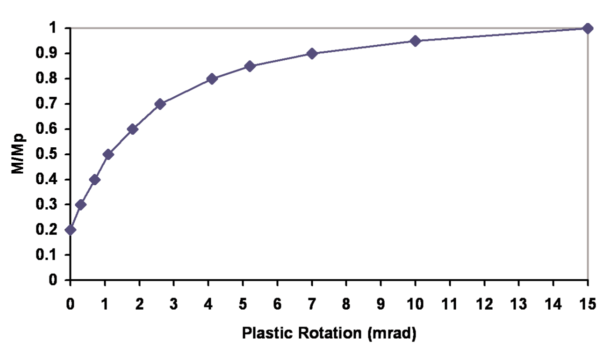

Fig. 4. Texas moment-rotation curve.

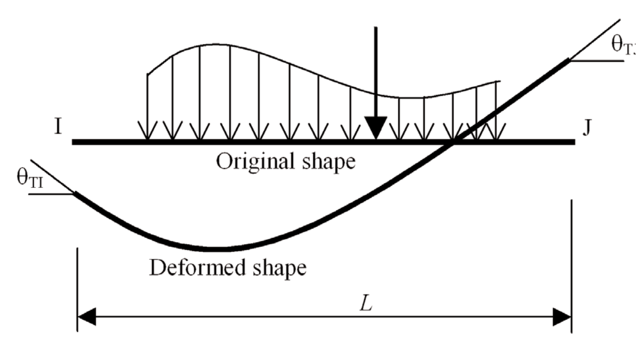

Fig. 5. Idealized deformation of a typical beam element.

and θ_{TJ} is the total rotation at end J, and L is the element length.

The method assumes that the function describing the relationship between φ (plastic section curvature) and M (moment) is monotonously increasing. By assuming that this function is valid for all sections of the beam element, the total rotation of this element can be calculated by:

$$\theta_{TI} + \theta_{TJ} = \int_0^L \varphi_T \, dx \tag{1}$$

θ_{TI} and θ_{TJ} are the total rotations at ends I and J, φ_T is the total section curvature, and L is the length of the element. The total section curvature consists of the summation of the elastic curvature, φ_e, and the plastic curvature, φ, such that:

$$\varphi_T = \varphi_e + \varphi \tag{1a}$$

Similarly, the total rotation consists of the summation of the elastic rotation, θ_e, and the plastic rotation, θ:

$$\theta_T = \theta_e + \theta \tag{1b}$$

By separating the plastic rotation θ from the elastic rotation, Equation 1 becomes:

$$\theta = \theta_I + \theta_J = \int_0^L \varphi \, dx \tag{2}$$

where φ represents the plastic curvature, and θ_I and θ_J are the plastic rotations at ends I and J.

The derivation detailed in Appendix A shows that the curvature φ for a point located at a distance x from the left end of the beam element may be expressed as a function of the applied moment, M, and the length of the beam element, L, by an expression of the form:

$$\varphi(M) = \begin{cases} \dfrac{1}{L}\left(\dfrac{M}{120} - 0.001\right) & \text{for } 0.2 \le x < 0.5 \\ \dfrac{1}{L}\left(\dfrac{M}{23} - 0.0186\right) & \text{for } 0.5 \le x < 0.8 \\ \dfrac{1}{L}\left(\dfrac{M}{2} - 0.3839\right) & \text{for } 0.8 \le x < 1.0 \end{cases} \tag{3}$$

This expression may be represented as shown in Figure 6.

Following the observation made by the researchers in Texas, we assume that the M-φ curve described in Figure 6 can be used to describe the behavior of most typical composite steel girder sections in positive bending.

Calculation of Plastic Rotations at Beam Element Ends

Following the derivations shown in Appendix A, and assuming that φ varies linearly along the element's length, the rotations, θ_I and θ_J, at the ends I and J of each beam element can be approximated as:

$$\begin{aligned} \theta_I &= \varphi_I \frac{L}{2} \\ \theta_J &= \varphi_J \frac{L}{2} \end{aligned} \tag{4}$$

Thus, the model approximates the effect of member plasticity by assuming that it is evenly spread over an equivalent plastic hinge length $L_{gp}=L/2$. When the beam element is long, or when the moment diagram within one element has large levels of fluctuations, the assumption that the curvature varies linearly is not valid as this assumption would result in a stiff beam element that will underestimate the "true" deformations. However, by refining the mesh and increasing the number of elements used to model the bridge superstructure, the results obtained will approach the actual results. Hence, assuming a linear variation of curvature along an element length is consistent with the finite element methodology.

Calculation of the Plastic Hinge Stiffness Coefficients, β_I and β_J

In this study we assume that the rotations at ends I and J of a beam element are related to the moments at these ends by the stiffness coefficients β_I and β_J. From Figure 2 and knowing θ_I and θ_J from Equation 4, the stiffness coefficients β_I and β_J can be calculated as:

$$\beta_I = \frac{\Delta\theta_I}{\Delta M_I}; \quad \beta_J = \frac{\Delta\theta_J}{\Delta M_J} \tag{5}$$

θ_I and θ_J are the end rotations calculated as shown in Equation 4 from the moment-curvature relationship of Equation 3. The rotational spring stiffness coefficients β_I and β_J are used as input to the stiffness matrices described in Figure 3.

IMPLEMENTATION

Nonlinear Bridge Analysis (NONBAN) was written to perform the nonlinear analysis of bridge systems using the grillage analysis method described in this paper. NONBAN also uses an incremental loading technique to simulate the nonlinear structural behavior of a girder bridge under applied vehicular loads. The objective of NONBAN is to describe the failure path of composite steel girder bridges. To use NONBAN, the bridge should be discretized as a plane grid (grillage model) with composite (or noncomposite) longitudinal elements representing the main girders and transverse beam elements representing the slab and diaphragms that contribute to the lateral distribution of the load to the longitudinal members. In NONBAN, all members, longitudinal or transverse, may exhibit nonlinear behavior.

Nonlinear member properties are considered for bending about the main axis of each element and for shear deformations in the vertical direction. The nonlinear behavior of each element is modeled by a multilinear moment versus plastic rotation (M-θ) curve and a multilinear shear deformation (V-γ) curve as shown in Figure 2. The slopes of the moment versus plastic rotation curve are calculated as described in the previous section. For typical steel bridges, the shear deformations are negligible and may be ignored. The rest of the input is similar to the input required for any linear elastic analysis of composite steel frames. Hambly (1991) and Zokaie et al. (1991) give a full description of the linear-elastic properties required to perform the grillage analysis. The input consists of the moment of inertia for every beam element (including polar moment of inertia to account for the torsional effects), the elastic and shearing moduli as well as the distributed dead load and the nodal location of the applied live load. In NONBAN, the live load is automatically incremented throughout the linear and nonlinear ranges until failure is reached. Failure is defined as the formation of a mechanism (instability of the system) or as the load at which a maximum deflection or maximum beam rotation is reached. The output of the program includes the deflections, the total rotations at each node, and the moments and forces at the ends of each beam element. The output also consists of a plot giving the load factor versus deformation curve that describes the relationship between the amplitude of the applied live load and the maximum vertical displacement of the bridge. A complete user manual and a listing of the program are provided in the Appendix to NCHRP Report 12-36 (Ghosn, Deng, Xu, Liu, and Moses, 1997). The program was found to provide acceptable agreements with the results of experimental tests on full-scale and model-scale composite steel girder bridges as will be discussed in the next section.

MODEL VERIFICATION

The verification of the program NONBAN and the modeling scheme proposed in this paper to study steel I-beam bridges is accomplished by comparing the results of NONBAN to those of a full-scale laboratory test and a model-scale test. The full-scale test was performed in the Structural Laboratory of the University of Nebraska (Kathol, Azizinamini, and Luedke, 1995) while the mode test was performed in Canada (Razaqpur and Nofal, 1988).

Nebraska's Full Scale Bridge Test

The bridge was designed, constructed and tested in the Structural Laboratory of the University of Nebraska-Lincoln for a project sponsored by the Nebraska Department of Roads (Kathol et al., 1995). The test was performed on a full-scale bridge model having a span of 70 ft and width of 26 ft. The superstructure consists of three welded plate girders built compositely with a 7 ½ in. reinforced concrete deck. The girders are spaced 10 ft on center and the reinforced concrete deck has a 3 ft overhang. Figure 7 shows this bridge's cross-section. The plates forming the girders consist of a 9 in. × ¾ in. top flange, a 54 in. × ⅜ in. web, a 14 in.×1 ¼ in. center bottom flange, and 14 in.× ¾ in. end bottom flange. Intermediate web stiffeners consist of a total of four 5⁄16 in. thick plates spaced at 39.5 in. and 10 plates at 67.2 in. Shear studs ⅞ in. in diameter and 5 in. tall are spaced 18 at 7 in., 14 at 9 in. and 16 at 10 3⁄16 in. from left to right. The studs are placed symmetrically about the girder centerline.

During bridge construction, cross-frames ("K-Frame" types) were placed at 11.2-ft spacings. For the ultimate load test, the cross-frames were removed and the bridge was loaded in both lanes simultaneously until failure. The bridge failed when shear punching occurred under one loading point in the slab. Figure 8 shows the loading configuration used by Kathol et al. (1995). These loads simulate two

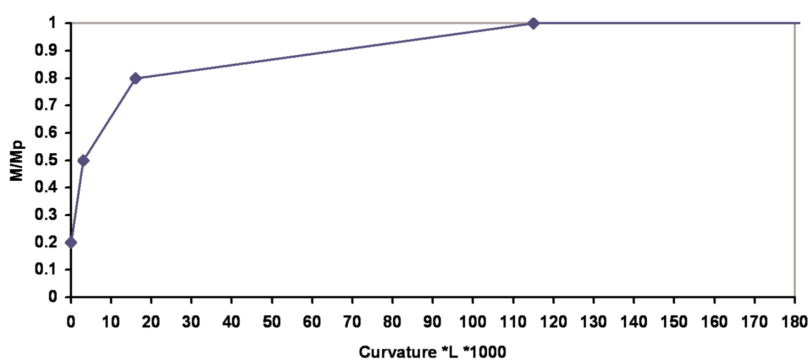

Fig. 6. Idealized moment curvature relationship using four linear segments.

side-by-side vehicles having configurations similar to one HS-20 truck in each lane.

To obtain the material properties, strength tests were performed on steel samples and concrete cylinders. The average results of these tests are summarized in Table 1, which is adapted from the reference by Kathol et al. (1995).

To perform the structural analysis using the approach proposed in this study, the bridge is modeled as a grid as shown in Figure 9. Each longitudinal girder is divided into 10 equal elements. The contribution of the slab to the longitudinal strength and stiffness is considered by using the properties of the composite section. The contribution of the slab to the transverse distribution of the load is effected by 11 transverse beams. The points of application of the wheel loads are represented by the symbol "■" in Figure 9. Since these points do not correspond to actual nodes on the grid model, nominal (artificial) elastic beams with negligible stiffness are used to connect these points to the adjacent nodes.

Elastic and inelastic member properties are calculated for all beam sections. The longitudinal girders' composite moment of inertia is found to be 66,955 in.^{4}. The ultimate moment capacity is 77,493 kip-in. for positive bending. The bare steel section produces a moment of inertia of 21,332 in.^{4} and the ultimate moment capacity is 35,988 kip-in. The middle transverse beam representing the contribution of an 83 in. wide portion of the slab has a moment of inertia equal to 2,980 in.^{4}, the torsion coefficient, J_x, is

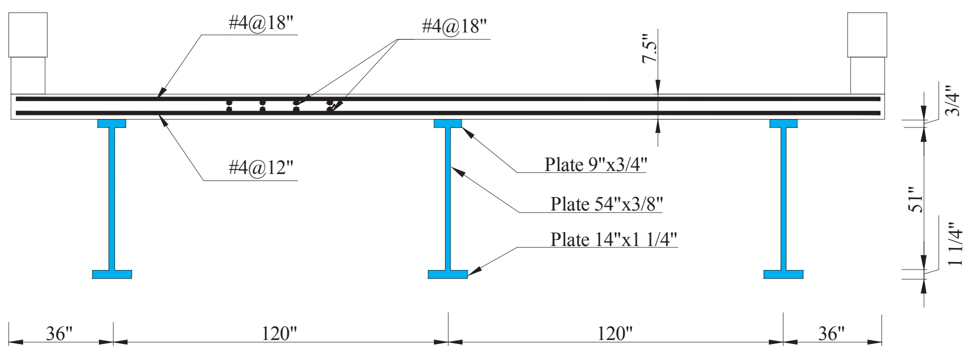

Fig. 7. Cross section of Nebraska bridge.

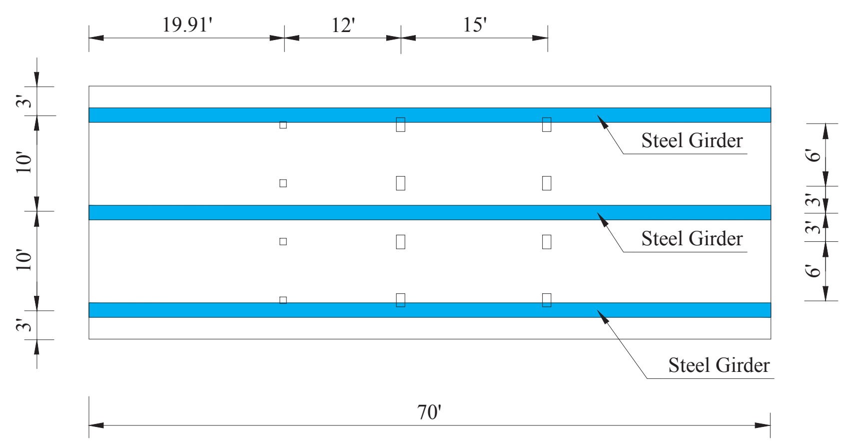

Figure 8. Loading configuration of Nebraska bridge simulating two HS-20 trucks in each lane.

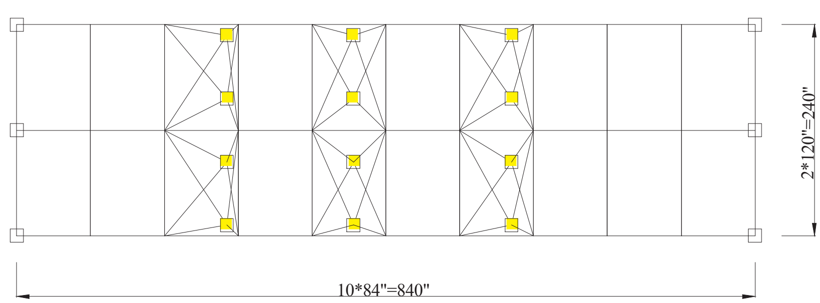

Figure 9. Grid mesh used to model the Nebraska bridge.

Table 1. Summary of Material Strengths for the Nebraska Bridge			
Material	Yield Stress f_y (ksi)	Ultimate Stress (ksi)	Young's Modulus E (ksi)
Structural Steel	41.73	65.56	27,600
Reinforcing Bars	72.6	119.35	27,550
Concrete	–	6.151	4,470

5,840 in.^{4} (from $J_x = bt^3/6$ as proposed by Hambly, 1991) and the ultimate moment capacity is 746 kip-in. The end transverse beams have a moment of inertia and ultimate moment capacity equal to one half those of the middle beams. The moment curvature relationship of the concrete transverse beams is obtained using concrete beam theory.

The dead load is divided into a permanent dead load and a superimposed load. The permanent dead load applied on the bare section is equal to 0.092 kip/in. The superimposed dead load applied on the composite girders is 0.023 kip/in.

Tests to determine the ultimate load capacity of the bridge were performed by applying various levels of loads through hydraulic jacks (Kathol et al., 1995). The loads were increased until punching shear failure occurred in the slab under one of the load pads. The researchers observed that: "The girders remained elastic until a load level equal to 12 times the weight of HS-20 trucks... The location of the neutral axis did not change throughout the loading process indicating that composite action remained at very high load levels." Punching shear failure in the slab occurred at a load level corresponding to 16 times that of HS-20 trucks. The

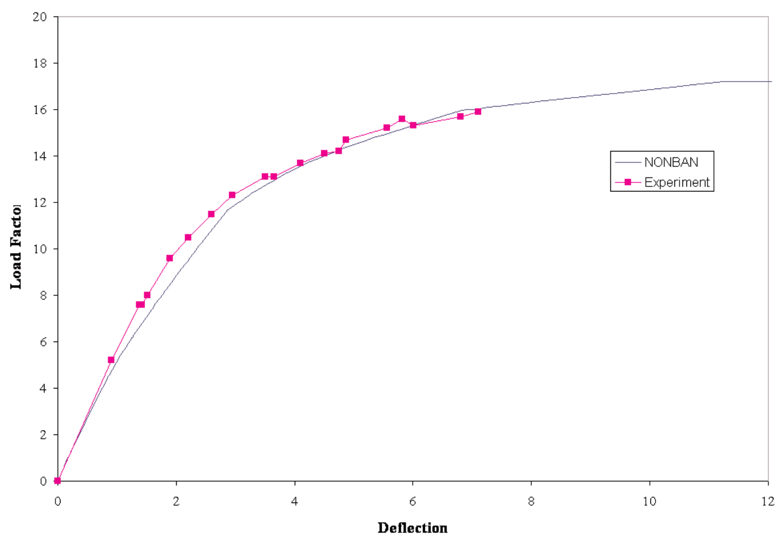

Fig. 10. Comparison of results between NONBAN and the experiment for Nebraska bridge.

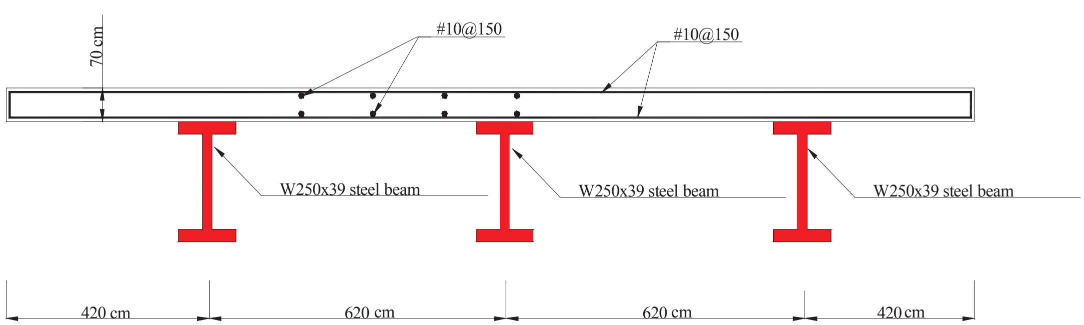

Fig. 11. Cross section of Canada's model bridge.

deflection at that load level was measured to be approximately 7.1 in. Although the load deflection curve was beginning to flatten out at that point, it was evident that the ultimate capacity of the main girders was not reached (Kathol et al., 1995).

The program NONBAN is run assuming that the sections are composite and accounting for the different properties of the edge beams and interior beams. For the edge beams however, the effect of the railings was ignored. Since the middle diaphragms were removed before the ultimate load test, the NONBAN model ignored their presence. Also, the model ignored the presence of the edge diaphragms since their contribution at this point is mainly for stability of the loaded structure. NONBAN used the Texas curve to model the behavior of the composite compact sections in positive bending (Equation 3 and Figure 6).

Figure 10 shows a comparison between the laboratory results (Kathol et al., 1995) and the results of NONBAN. Reasonably good agreement is observed in the figure for the whole range of the loading process including the prediction of the yielding load and the nonlinear loading path. The result shows that the ultimate capacity was not reached in the test but that the slab punching shear failure occurred at a load level slightly lower than ultimate. Because accurate models to predict the punching shear capacity of bridge decks were not available NONBAN was run without considering the possibility of punching shear failures. If no limits on member ductility are assumed and ignoring shearing failures, NONBAN predicted that the ultimate load would be reached at a load factor corresponding to 17.21 times the two HS-20 trucks. This corresponds to the formation of a mechanism which is manifested by obtaining large levels of deformation for a very small increment of load.

Canada's Bridge Model Test

The Canadian laboratory test (Razaqpur and Nofal, 1988) was performed on a model of a simple span bridge with a span length equal to six meters. The bridge consists of three steel W250×39 rolled I-beams with a 6000 mm span supporting a 70 mm deck slab as shown in Figure 11. Core samples were used to estimate the strength of the concrete in the deck and the steel of the beams. The beams and the slab were built to act as composite sections. The bridge model did not have any midspan cross frames or diaphragms. The material properties are given in Table 2.

Tests to determine the ultimate load capacity of the bridge were performed using an actuator. The loads simulated a three-axle truck configuration. The loads were applied at three points above the middle girder as described by Razaqpur and Nofal (1988) and shown in Figure 12. The loads were then increased until the ultimate capacity was reached. To prepare the mesh for the NONBAN analysis, the length of the bridge is again divided into ten equal segments. The longitudinal beams are connected by eleven transverse beams representing the transverse capacity of the slab.

Figure 13 shows a comparison between the laboratory results published by Razaqpur and Nofal (1988), and the results of NONBAN. Reasonably good agreement is observed in the figure for the whole range of loading including the prediction of the yielding load and the maximum load. It is observed that the NONBAN results produced an ultimate load of 719.5 kN. This value is similar to the maximum load measured in the laboratory, which is equal to 720 kN. This example gives an illustration of the validity of the program NONBAN and the proposed method to model the nonlinear behavior of steel members.

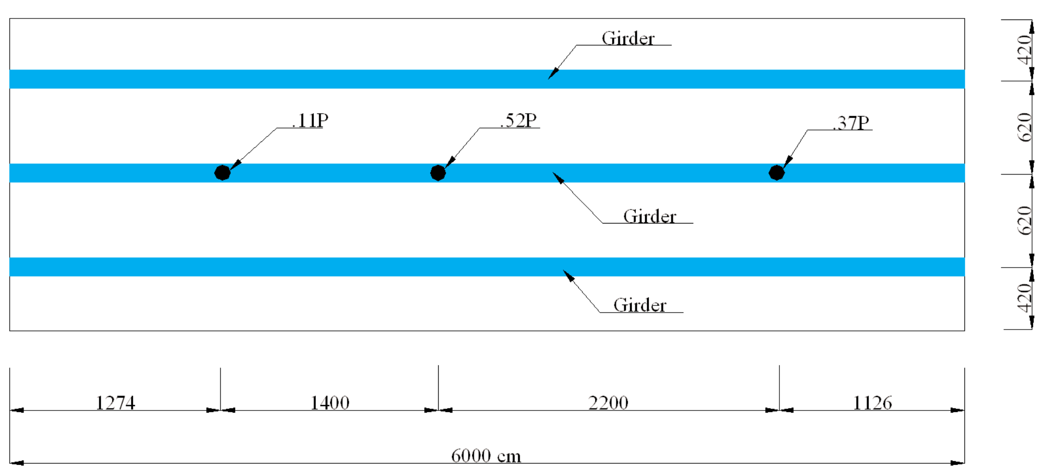

Fig.12. Load positions used during ultimate capacity testing of Canada bridge.

Table 2. Material Properties for the Canada Bridge						
Material	f'_c (MPa)	f'_t (MPa)	σ_y (MPa)	ε_y	ε_u	E (GPa)
Concrete	42.1	3.5	–	0.0005	0.0045	31
Rebar	–	–	400	0.002	0.02	200
Structural Steel	–	–	300	0.002	0.02	150

SENSITIVITY OF RESULTS TO MESH-SIZE

From experimentation with the grid method it has been observed that there are two factors that may affect the results of the nonlinear analysis. The first one is the stopping criterion (i.e. the definition of failure). The second one is the stability of the mesh size. Several stopping criteria have been used with NONBAN. These include:

1. The formation of a plastic hinge mechanism.
2. A large level of deflection rendering the bridge non-functional.
3. A maximum plastic hinge rotation in a beam element causing the element to unload.
4. Punching shear failures.

In many practical situations criteria 2, 3 and 4 may occur before a mechanism forms. Criterion 2 implies a certain level of subjective judgement in order to define the level of displacement that would render a bridge nonfunctional. Ghosn and Moses (1998) have used a maximum deflection of span length/100 to define the functionality limit state. In addition, most experimental investigations on bridge structures have shown that punching shear failures normally occur in secondary members (e.g. slab), thus eliminating the need to use criterion 4 for most practical situations as this implies a local failure rather than the collapse of the bridge. Criterion 3 implies that a bridge is considered to have failed when the plastic rotation in a main load-carrying member reaches a limiting value. The limiting rotation value is normally obtained from experimental results depending on the materials properties (e.g. composite member failure occurs when the strain in concrete reaches its ultimate value causing the crushing of concrete or when the steel fractures as it reaches its tensile capacity). Schilling and Morcos (1988) have shown that steel composite girders in positive bending have very high ductility levels. This would justify the unlimited ductility assumption used during the analyses of the two simple span bridges mentioned above although NONBAN can accept any limits that the operator chooses to use. For negative bending, limits in the

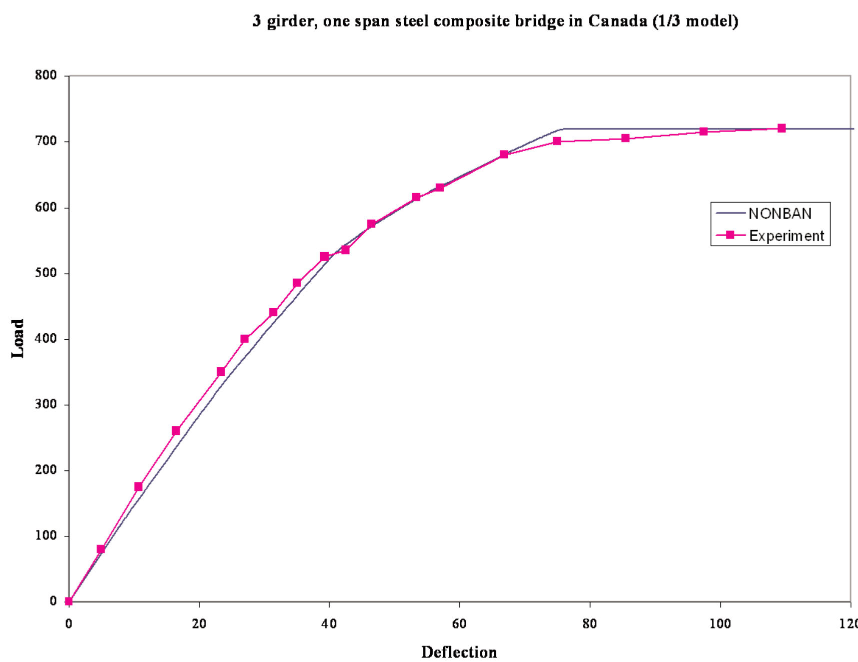

Fig. 13. Comparison of NONBAN results to experiment results of Canada bridge.

ductility levels and a description of the unloading behavior are provided by Schilling and Morcos (1988) for sections of different depth to thickness (slenderness) ratios.

Based on their experience with the grillage analysis of elastic bridges, Hambly (1991) and Zokaie et al. (1991) have recommended to discretize bridges into 10 equal elements in the longitudinal direction to obtain good results during the linear elastic analysis. The experience of the writers confirm this recommendation even for the nonlinear analysis as long as the moment rotation relationship used during the analysis is obtained from experimental results and is used as recommended in this paper. This recommendation is made based on several successful comparisons between the results of NONBAN and those of published experimental tests. As an illustration of the robustness of the proposed mesh discretization procedure, the results obtained by NONBAN for different mesh sizes are compared to those of the experimental data for the bridge test performed in Nebraska. Figure 9 shows the mesh of the base case that divided the longitudinal girders into ten equal beam elements. The results obtained show good agreement with the test results as illustrated in Figure 10. If the mesh size is changed such that the longitudinal girders are divided into 5, 20 or 40 equal elements, the final results are as good as those of the base case as shown in Figure 14. It is noted however, that the change in the mesh size did produce some difference in the final failure point. The cause of this difference is in the approximation used during the derivation of Equation 4. This difference is manifested by having different displacements at failure while the ultimate loads obtained from the different meshes show minor differences.

CONTINUOUS STEEL BRIDGES

Continuous steel bridges whose members exhibit both positive as well as negative bending can be analyzed using the same approach described above. The negative bending moment-curvature relationship, M-φ, curve can be obtained from experimental moment-plastic rotation, M-θ, curves using steps similar to those described in Appendix A. Experimental M-θ curves for compact, ultracompact, and noncompact sections in negative bending are available in the literature. For example, Schilling (1989) provides such curves for different section slenderness ratios. For a low slenderness ratio, the experimental curve may be represented as shown in Figure 15.

Using the same definitions given above, the curve in Figure 15 can be expressed as:

$$\theta = (16.67M - 11.67) \quad \text{for } 0.7 \leq x < 1.0 \tag{6}$$

resulting in the following expression for the plastic

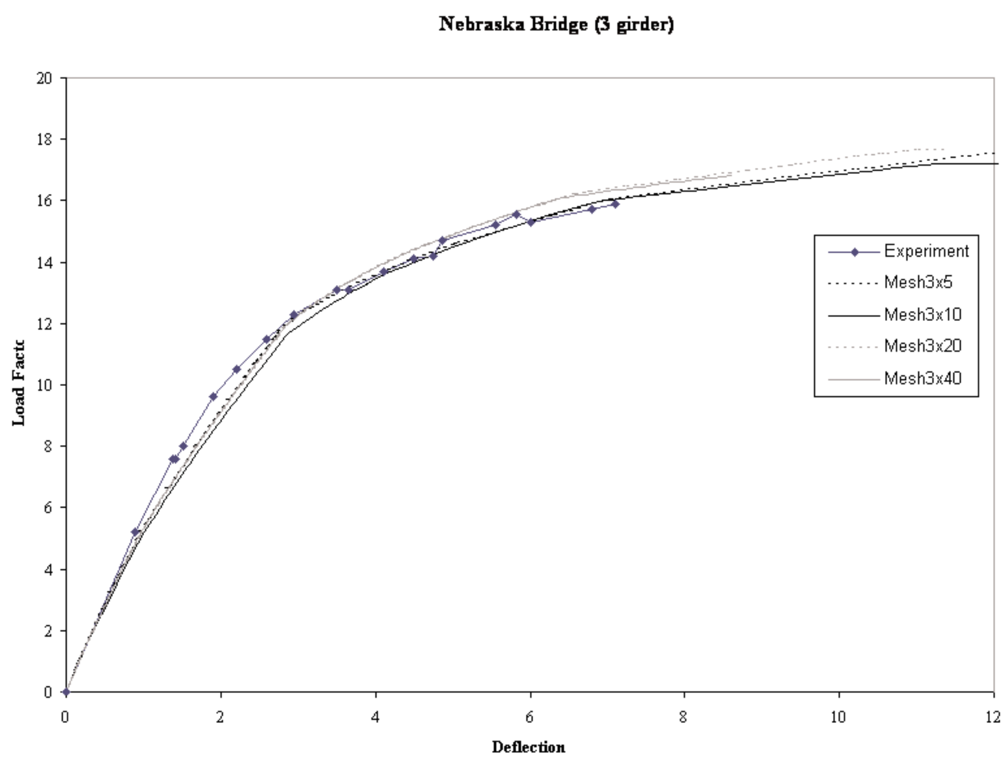

Fig.14. Results of Nebraska bridge for different mesh sizes compared to experiment results.

curvature:

$$\varphi(M) = \frac{1}{L}(33.33M - 11.67) \quad \text{for } 0.7 \leq x < 1.0 \tag{7}$$

Given the moment-curvature expressions of Equation 3 and Equation 7, the standard analysis procedure developed above can be used to analyze continuous steel girder bridges. The validity of the approach is demonstrated using the results of the Tennessee field test (Burdette and Goodpasture, 1971).

Tennessee Field Test

Burdette and Goodpasture (1971) performed the Tennessee field test on a four-span continuous bridge with span lengths of 70 ft, 90 ft, 90 ft, and 70 ft. The bridge consists of four steel W36×170 rolled I-beams at 8.25-ft spacings supporting a 7-in. deck slab. Sections over the piers are W36×160 with 10½ in.×1 in. cover plates at the bottom. The loads were placed to simulate an HS truck in each lane of the second span. Burdette and Goodpasture (1971) give a more complete description of the tested bridge. Core samples were used to estimate the strength of the concrete in the deck and the steel of the beams. The beams and the slab were built to act as composite sections.

Tests to determine the ultimate load capacity of the bridge were performed by anchoring a rod into the rock below the bridge and jacking. The loads were then increased until the ultimate capacity is reached. The researchers observed that:

> The first evidence of distress was related to the diaphragms when a noticeable and audible slip occurred between the diaphragm and the steel girders... The behavior of the bridge was almost linear elastic up to yielding of the section under the applied loads... At a load of about 650 kips, a crack occurred between the curb and slab near the first pier and tension cracks were visible in the deck over the pier... After yielding, the bridge "lifted

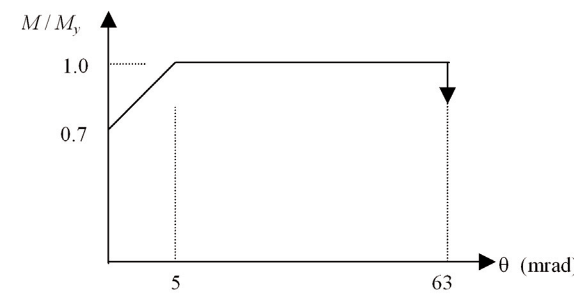

Fig. 15. M-θ curve for negative bending moment.

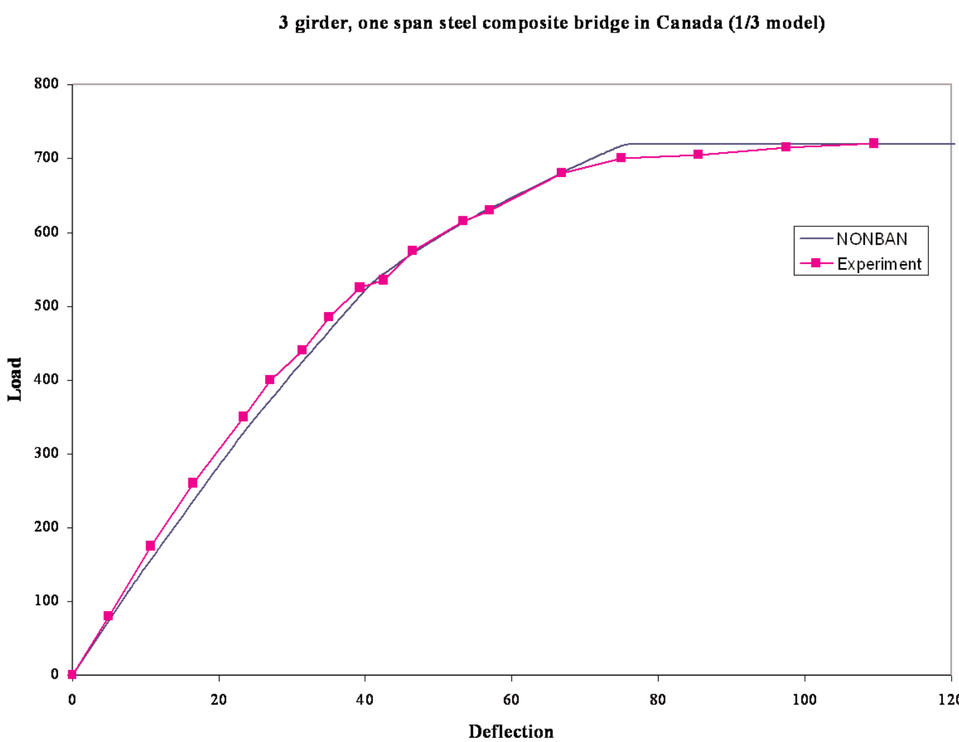

Fig. 16. Comparison of results of the experiment and NONBAN for four-span continuous Tennessee bridge.

> off' the abutment... Eventually, plastic hinges developed near the center pier and the web of the exterior girder buckled at the formation of the hinge.

Shortly after, compression failure occurred at one of the curbs and the test was terminated at a load of 125 kips.

The program NONBAN was run assuming that the contribution of the curbs and overhang to the properties of the longitudinal edge beams is similar to the effect of half the slab in the interior beams. Thus, all four longitudinal girders are assumed to have the same properties. Since the diaphragms broke early in the loading process, and since no information was provided about the properties of the diaphragms, the NONBAN model ignored their presence. For cases where the diaphragms are important, NONBAN can account for the their nonlinear behavior all the way until failure. To prepare the mesh for the NONBAN analysis, each span is divided into ten equal segments. The NONBAN analysis used the composite properties of the longitudinal beams for regions of positive bending. In the negative bending regions, the beam properties assume non-composite action but include the effect of the cover plates and the reinforcing steel of the slab. Since the amount of reinforcing steel was not provided in the reference, typical values were used. In this case it is assumed that the area of reinforcing steel is 3226 mm^2. The longitudinal beams are connected by forty-one transverse beams representing the transverse capacity of the slab. The possibility of having shear failures in the slab is not considered in this example.

Figure 16 shows a comparison between the field results published by Burdette and Goodpasture, (1971) and the results of NONBAN. Reasonable agreement is observed in the figure for the whole range of the loading process. This includes the prediction of the yielding loads and the ultimate load. In this analysis, bridge members are assumed to have an infinite level of ductility in positive bending, and the ultimate capacity is reached when a mechanism forms which is manifested by obtaining large levels of deformation for a very small increment of load. This example demonstrates the validity of the proposed model and the program NONBAN to perform the nonlinear analysis of typical continuous steel bridges as well as simple span bridges. The method requires valid moment-curvature relationships that accurately represents the behavior of girder sections for the bridges being analyzed. For bridges with unusual designs, the Texas and Schilling curves used in this paper may not be applicable, and additional research may be required to verify these curves' validity for such cases before applying them in conjunction with the model proposed in this paper.

CONCLUSIONS

This paper described a method to analyze the nonlinear response of steel girder bridges. The method has the following features:

- It is based on a nonlinear grillage analysis using an incremental loading technique to derive a complete load versus deflection curve.
- The input data is similar to that required for the linear analysis of bridges. This data consists of the bridge geometry (mesh) as well as the linear elastic properties of the members (moments of inertia, modulus of elasticity, etc.). The only additional input data required is the ultimate moment capacity of each section M_p and shear capacity as well as the moment versus curvature, and shear versus shearing strain relationships.
- The method can predict the load path realistically both for simple-support and continuous bridges. Particularly, reasonably accurate results are obtained when the moment curvature relationship is derived from experimental steel beam tests such as the ones conducted at the University of Texas.
- The method provides a simple tool that can be used to obtain detailed descriptions of the nonlinear behavior and ultimate capacity of highway bridges.
- The validity of the model was verified by comparing the results to those from in-situ experimental tests and from full scale and model scale laboratory tests.
- The model that is proposed in this paper could be used to predict the complete nonlinear behavior of straight steel I-girder bridges. Such information may be useful for designing new bridges for ultimate limit states and for the rating of existing bridges. Taking advantage of the complete nonlinear behavior of bridges during the rating process may result in a reduction in the retrofitting needs.
- Because the model produces a complete load versus deformation curve for each bridge structure, the bridge designer (or rater) would be able to check the deflection of a bridge at different load levels to ensure that the bridge remains functional at high live loads. Independent checks of the serviceability limit states may still be necessary for certain applications.

ACKNOWLEDGMENTS

The work described herein was initiated during the study conducted by the authors and their colleagues as part of NCHRP project 12-36. The authors acknowledge the contributions of Mr. Charles Schilling, and Dr. Fred Moses. The original version of the program, NONBAN, used in this study was developed by Dr. Y. Liu formerly a research associate at Case Western Reserve University and Mr. Jimmy

Xu, research assistant at the City College of New York. The authors are also grateful for the contributions of Prof. J.R. Casas from the Technical University of Catalunya, PUC, Spain and the partial support provided by the Generalitat of Catalunya during the second author's sabbatical at PUC. The opinions and conclusions expressed or implied in this paper are those of the authors. They are not necessarily those of the Transportation Research Board or the Federal Highway Administration or the individuals participating in the National Cooperative Highway Research Program, NCHRP.

APPENDIX A. DERIVATIONS

Derivation of Moment-Curvature Relationship

The step function $\chi\ (M_i, M_j)$ is defined as:

$$\chi(M_i, M_j) = \begin{cases} 1 & M_i \le x \le M_j \\ 0 & \text{otherwise} \end{cases} \tag{A.1}$$

The relationship between the maximum moment applied on a beam segment, M, and the plastic rotation, θ, shown in Figure 2a can be expressed as:

$$\theta = \sum_{i=1}^{n} (\mathrm{a}_i + \mathrm{b}_i M)\chi(M_{i-1}, M_i) \tag{A.2}$$

n is the total number of linear segments used to model the moment-rotation relationship. a_i and b_i are constants giving the intercept and the slope of a linear equation. Thus, if ten segments are used to model the Texas curve, it can be represented by an expression of the form:

$$\begin{aligned} \theta = {} & (3M-0.6)\chi(0.2,\ 0.3) + (4M-0.9)\chi(0.3,\ 0.4) \\ & + (4M-0.9)\chi(0.4,\ 0.5) + (7M-2.4)\chi(0.5,\ 0.6) \\ & + (8M-3.0)\chi(0.6,\ 0.7) + (15M-7.9)\chi(0.7,\ 0.8) \\ & + (18M-10.3)\chi(0.8,\ 0.85) + (36M-25.4)\chi(0.85,\ 0.9) \\ & + (60M-47)\chi(0.9,\ 0.95) + (100M-85)\chi(0.95,\ 1.0) \end{aligned} \tag{A.3}$$

The following three observations were made by researchers while conducting the experiments that produced the Texas curve of Figure 4 (Vasseghi and Frank, 1987; Schilling, 1989):

- Plastic behavior begins at a moment level on the order of 0.2 times the plastic moment capacity (0.2 M_p).
- A plane section remains plane throughout the whole loading process.
- The Texas curve can be used to describe the behavior of most typical girders in positive bending for different span lengths and for different composite steel girder sections.

These three observations will be used as postulates during the derivations of the end stiffnesses for beam elements under nonlinear bending and as the basis for the calculations performed in this appendix.

The experimental set up used to generate the Texas curve and the corresponding bending moment diagram is modeled as shown in Figure A.1. In Figure A.1, the following symbols are used: x gives the location of the section under consideration, x_1 is the coordinate of the point where the plastic zone begins and x_2 is the coordinate of the point where the plastic zone ends. M_p is the ultimate capacity of a section. M is the moment at midspan ($0.2M_p \le M \le M_p$). m is the moment at point x.

According to Figure A.1, Equation 2 and the third postulate made above, this beam's plastic rotation θ can be expressed as a function of the section's plastic curvature, φ through an equation of the form:

$$\theta = \int_{x_1}^{x_2} \varphi dx; \text{ or, using symmetry,} \quad \theta = 2\int_{x_1}^{L/2} \varphi\, dx \tag{A.4}$$

Knowing that the nonlinear range begins at a moment level equal to 0.2 M_p through the first postulate, and given a linear moment diagram, the x_1 and x_2 coordinates can be calculated as:

$$x_1 = \frac{0.2M_p}{M}\frac{L}{2}, \text{ and by symmetry, } x_2 = L - x_1 \tag{A.5}$$

Substituting the expressions for x_1 and x_2 and Equation A.2 into Equation A.4, we obtain:

$$2\int_{\frac{0.2M_p}{M}\frac{L}{2}}^{\frac{L}{2}} \varphi dx = \sum_{i=1}^{n} (\mathrm{a}_i + \mathrm{b}_i M)\chi(M_{i-1}, M_i) \tag{A.6}$$

The curvature, φ, is a function of the moment, m. From Figure A.1, we know that:

$$x = \frac{L}{2}\frac{m}{M} \tag{A.7}$$

and

$$dx = \frac{L}{2}\frac{dm}{M} \tag{A.8}$$

Substituting Equations A.7 and A.8 into Equation A.6, we obtain:

$$\int_{0.2M_p}^{M} \varphi(m) dm = \frac{M}{L}\sum_{i=1}^{n} (\mathrm{a}_i + \mathrm{b}_i M)\chi(M_{i-1}, M_i) \tag{A.9}$$

Taking the derivatives of both sides of equation (A.9), the following expression for the curvature is obtained:

$$\varphi(M)=\frac{1}{L}\sum_{i=1}^{n}(\mathrm{a}_i+2\mathrm{b}_iM)\chi(M_{i-1},M_i) \qquad \text{(A.10)}$$
$$+\frac{1}{L}\sum_{i=1}^{n}\left[(\mathrm{a}_iM_{i-1}+\mathrm{b}_iM_{i-1}^2)\delta(M-M_{i-1})\right.$$
$$\left.-(\mathrm{a}_iM_i+\mathrm{b}_iM_i^2)\delta(M-M_i)\right]$$

For the example where the Texas moment rotation curve is represented by 10 linear segments, (n=10), Equation A.10 is expressed as:

$$\varphi(M)=\frac{1}{L}\left[(6M-0.6)\chi(0.2,\ 0.3)+(8M-0.9)\chi(0.3,\ 0.4)\right.$$
$$+(8M-0.9)\chi(0.4,\ 0.5)+(14M-2.4)\chi(0.5,\ 0.6)$$
$$+(16M-3.0)\chi(0.6,\ 0.7)+(30M-7.9)\chi(0.7,\ 0.8)$$
$$+(36M-10.3)\chi(0.8,\ 0.85)+(72M-25.4)\chi(0.85,\ 0.9)$$
$$\left.+(120M-47)\chi(0.9,\ 0.95)+(200M-95)\chi(0.95,\ 1.0)\right]$$
$$+\frac{1}{L}\sum_{i=1}^{n}\left[(\mathrm{a}_iM_{i-1}+\mathrm{b}_iM_{i-1}^2)\delta(M-M_{i-1})\right.$$
$$\left.-(\mathrm{a}_iM_i+\mathrm{b}_iM_i^2)\delta(M-M_i)\right] \qquad \text{(A.11)}$$

The function $\delta(M\text{-}M_i)$ is the dirac delta function defined as:

$$\delta(M-M_i)=\begin{cases}\text{undefined when } M=M_i\\ 0 \quad\quad \text{when } M\neq M_i\end{cases} \qquad \text{(A.12)}$$

$$\text{and} \quad \int_{-\infty}^{\infty}\delta(M-M_i)dM=1$$

The curvature expression of Equation A.11 can be graphed as shown in Figure A.2.

For simplicity, we can reduce the number of linear segments from 10 to 4 using a regression analysis through the points of Figure A.2. The following expression for M-φ is thus obtained:

$$\varphi(M)=\frac{1}{L}\sum_{i=1}^{3}(\mathrm{c}_i+\mathrm{d}_iM)\chi(-M_{i-1},M_i)$$
$$=\frac{1}{L}\left[\left(\frac{M}{120}-0.001\right)\chi(0.2,0.5)\right.$$
$$+\left(\frac{M}{23}-0.0186\right)\chi(0.5,0.8) \qquad \text{(A.13)}$$
$$\left.+\left(\frac{M}{2}-0.3839\right)\chi(0.8,1.0)\right]$$

This expression may be represented as shown in Figure 6 in the body of the text.

Following the third postulate made from the results of the Texas experiment, we assume that the M-φ curve shown in Figure 6 can be used to describe the behavior of most typical composite steel girder sections in positive bending.

Calculation of Plastic Rotations at Beam Element Ends

The distribution of the plastic curvature φ along the length, L, of a beam element may be represented as a multi-linear curve as shown in Figure A.3. The amplitude of the curvature depends on the element's moment distribution following the expression of Equation A.13.

In Figure A.3, φ_i, is the plastic curvature at point i (i = 0,…,k, where i = 0 at end I and i = k at end J) and L_j (j = 1, 2, …k) is the length of segment j. Based on Figure A.3, the plastic rotation θ of a beam segment of length L ($L = \sum L_j$) is:

$$\theta=\theta_{\mathrm{I}}+\theta_{\mathrm{J}}=\sum_{i=1}^{k}\int_0^{L_i}\left(\varphi_{i-1}+\frac{\varphi_i-\varphi_{i-1}}{L_i}x\right)dx$$
$$=\sum_{i=1}^{k}\left(\varphi_{i-1}+\varphi_i\right)\frac{L_i}{2} \qquad \text{(A.14)}$$

θ_{I} is the plastic rotation at end I, and θ_{J} is the plastic rotation at end J. For simplification and without losing generality, we can assume that the rotation at end I is related to the curvature at point I and the plastic rotation ($\theta_{\mathrm{I}}+\theta_{\mathrm{J}}$) of the beam by:

$$\theta_{\mathrm{J}}=\frac{\varphi_{\mathrm{J}}}{\varphi_{\mathrm{I}}+\varphi_{\mathrm{J}}}\left(\theta_{\mathrm{I}}+\theta_{\mathrm{J}}\right)$$
$$=\frac{\varphi_{\mathrm{J}}}{\varphi_{\mathrm{I}}+\varphi_{\mathrm{J}}}\sum_{i=1}^{k}\left(\varphi_{i-1}+\varphi_i\right)\frac{L_i}{2} \qquad \text{(A.15)}$$

Similarly, the rotation at end J is related to the total rotation and the curvature at J by:

$$\theta_{\mathrm{J}}=\frac{\varphi_{\mathrm{J}}}{\varphi_{\mathrm{I}}+\varphi_{\mathrm{J}}}\left(\theta_{\mathrm{I}}+\theta_{\mathrm{J}}\right)$$
$$=\frac{\varphi_{\mathrm{J}}}{\varphi_{\mathrm{I}}+\varphi_{\mathrm{J}}}\sum_{i=1}^{k}\left(\varphi_{i-1}+\varphi_i\right)\frac{L_i}{2} \qquad \text{(A.16)}$$

For simplicity, assume that φ varies linearly along the element's length, that is, there is only one linear segment between points I and J. By letting k = 1 in Equations A.15 and Equation A.16, we obtain:

$$\theta_{\mathrm{I}}=\varphi_{\mathrm{I}}\frac{L}{2}$$
$$\theta_{\mathrm{J}}=\varphi_{\mathrm{J}}\frac{L}{2} \qquad \text{(A.17)}$$

When the beam element is long, or when the moment diagram within one element has large levels of fluctuations, the assumption that the curvature varies linearly is not valid as this assumption would result in a stiff beam element that will underestimate the "true" deformations. However, by refining the mesh and increasing the number of elements used to model the bridge superstructure, the results obtained will approach the actual results. Hence, assuming a linear variation of curvature along an element length is consistent with the finite element methodology.

Calculation of the Plastic Hinge Stiffness Coefficients, β_I and β_J

In this study we assume that the rotations at ends I and J of a beam element are related to the moments at these ends by the stiffness coefficients β_I and β_J. From Figure 2 and knowing θ_I and θ_J, from Equation A.17, the stiffness coefficients β_I and β_J can be calculated as:

$$\beta_I = \frac{\Delta\theta_I}{\Delta M_I},\ \beta_J = \frac{\Delta\theta_J}{\Delta M_J} \qquad \text{(A.18)}$$

θ_I and θ_J are the end rotations calculated as shown in Equation A.17 from the moment-curvature relationship of Equation A.13. The rotational spring stiffness coefficients β_I and β_J are used as input to the stiffness matrices described in Figure 3.

REFERENCES

AASHTO (1994), "AASHTO LRFD Bridge Design Specifications," American Association of State Highway and Transportation Officials.

Burdette, E. G. and Goodpasture, D. W. (1971), "Full Scale Bridge Testing - An Evaluation of Bridge Design Criteria," University of Tennessee, December.

Ghosn, M., Casas, J. R. and Xu, J. M. (1996), "Development of an Efficient Program for the Nonlinear Analysis of Bridges," *Journal of Computers and Structures*, Vol. 61, No. 3, pp. 459-470.

Ghosn, M., Deng, L., Xu, J. M., Liu, Y. and Moses, F. (1997), "Documentation of Program NONBAN," National Cooperative Highway Research Program, NCHRP 12-36, Transportation Research Board, National Research Council, Washington, D.C.

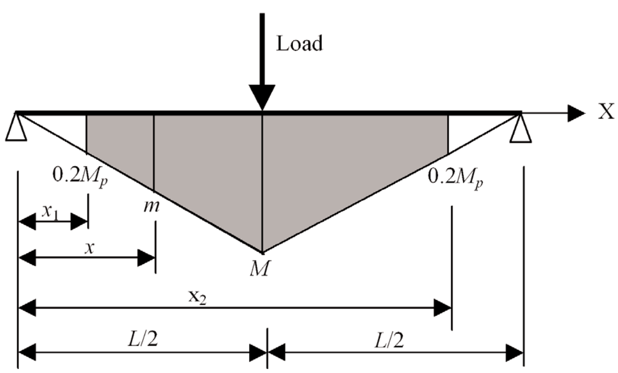

Fig. A.1. Moment diagram for Texas experiment set-up.

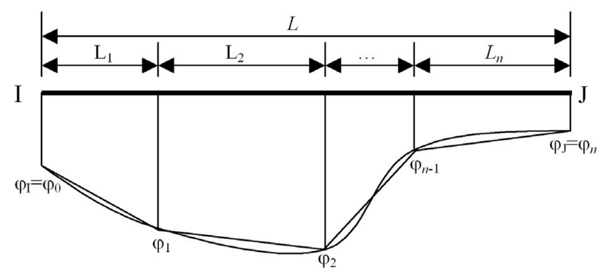

Fig. A.3. Multi-linear representation of a beam element's curvature.

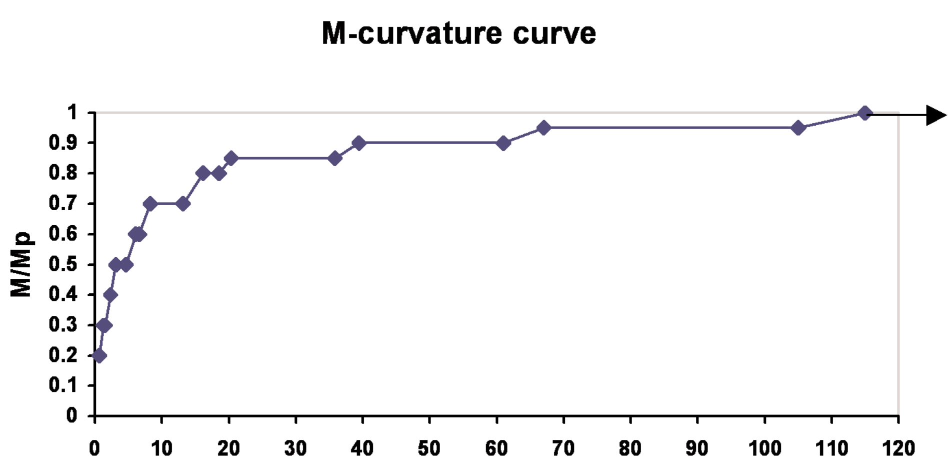

Fig. A.2. Plot of calculated moment-plastic curvature relationship.

Ghosn, M. and Moses, F. (1997), "Redundancy in Highway Bridge Superstructures," Final report, National Cooperative Highway Research Program, NCHRP 12-36, Transportation Research Board, National Research Council, Washington D.C.

Ghosn, M. and Moses, F. (1998), "Redundancy in Highway Bridge Superstructures," National Cooperative Highway Research Program, National Academy Press, Report No. 426, Washington, D.C.

Hall, J. C. and Kostem, C. N. (1981), "User's Manual for Program BOVAS," Fritz Engineering Laboratory Report No. 435.3A, Lehigh University, Bethlehem, PA.

Hambly, E. C. (1991), "Bridge Deck Behavior," E & FN Spon, London.

Hawkin, N. M. and Mitchell, D. (1984), "Seismic Response of Composite Shear Connections," *Journal of Structural Engineering*, ASCE, Vol. 110, No. 9, September.

Idriss, R. L., White, K. R. (1991), "Secondary Load Paths in Bridge Systems," Transportation Research Records No. 1290, TBR Bridge Engineering Conference, March, 1991.

Kathol, S., Azizinamini, A. and Luedke, J. (1995), "Strength Capacity of Steel Girder Bridges," NDOR Research Project No. RES1 90099, P469, Nebraska Department of Roads, February.

Keuser, M. and Mehlborn, G. (1987), "Finite Element Models for Bond Problem," *Journal of Structural Engineering*, ASCE, Vol. 113, No.10, October.

Komatsu, S., Moriwaki, Y., Fujino, M. and Takimoto, T., (1984), "Ultimate Strength of Girders in Combined Load," *Journal of Structural Engineering*, ASCE, Vol. 110, No. 4, April.

Kullman, R. B., Hosain, M. U. (1985), "Shear Capacity of Stub-Girders: Full Scale Tests," *Journal of Structural Engineering*, ASCE, Vol. 111, No. 1, January, pp. 56-75.

Livesley, R. K. (1970), "Matrix Methods of Structural Analysis," Pergamon, Oxford.

Nagarajarao, N. R., Estuar, F. R. and Tall, L. (1964), "Residual Stress in Welding Shapes," The Welding Journal, Research Supplement, Vol. 43, July, pp. 255-306.

Razaqpur, A. G. and Nofal, M. (1988), "Transverse Load Distribution at Ultimate Limit States in Single Span Slab-on-Girder Bridges with Compact Steel Girders," Ontario Ministry of Transportation, MISC-88-01, September.

Ricles, J. M., Yang, Y. S., and Priestley, M. J. (1998), "Modeling Nonductile R/C Columns for Seismic Analysis of Bridge," *Journal of Structural Engineering*, ASCE, Vol. 124, No. 4, April.

Ricles, J. M. and Popov, E. P. (1994), "Inelastic Link Element for EBF Seismic Analysis," *Journal of Structural Engineering*, ASCE, Vol. 120, No. 2, pp. 441-443.

Schilling, C. G. (1989), "A Unified Autostress Method," Project 51 (Development of Design Specifications for Continuous Composite Plate-Girder Bridges), American Iron and Steel Institute.

Schilling, C. G. and Morcos S. S. (1988), "Moment-Rotation Tests of Steel Girders with Ultracompact Flanges," Project 188 Autostress Design of Highway Bridges, American Iron and Steel Institute, 06.

Vasseghi, A. and Frank, K. H. (1987), "Static Shear and Bending Strength of Composite Plate Girders," Final Report AISI Laboratory Report N. 87-4, University of Texas, Austin, TX, June.

Zdenek, P., Bazant, F., and Byung, H. (1983), "Deformation of Cracked Net-Reinforced Concrete Walls," *Journal of Structural Engineering*, ASCE, Vol. 109 No. 1, January, pp. 93-108.

Zokaie T., Osterkamp, T. A., and Imbsen, R. A. (1991), "Distribution of Wheel Loads on Highway Bridges," Final Report, NCHRP project 12-2/1, March.